ISSN 1330-3651(Print), ISSN 1848-6339 (Online)
UDC/UDK [624.078.4:691.116]:519.6

PARAMETRIC ANALYSIS OF LARGE DIAMETER MECHANICAL FASTENER IN REINFORCED GLULAM

Krunoslav Pavković, Vlatka Rajčić, Dean Čizmar

Preliminary notes

Research deals with a 49 mm in diameter mechanical fastener in reinforced laminated timber, to which a load perpendicular to grain is applied. Influence of glass fibre textile to reinforcing connection zone on the joint mechanical properties was carried out. The experimental tests were divided in two stages: first stage was carried out on locally reinforced and second on non-reinforced timber specimens. Finite element models were made in software package Abaqus/CEA ver. 6.10. UMAT subroutine and surface-based cohesive behaviour were used for modelling complex timber behaviour. Results obtained by finite element model and experimental tests were shown and compared for non-reinforced and reinforced specimens with 900 g/m^2 of textile in connection zone. Also, parametric finite element model analyses were carried out for reinforced specimens with textile quantity between 0 ÷ 900 g/m^2 in the connection zone. Research results have shown that the application of textile in connection zone increases maximum force and yield force even in the smallest quantity.

Keywords: *glulam (glued laminated timber), large diameter fastener, mechanical fastener, reinforced timber joint, textile reinforcement, UMAT subroutine*

Parametarska analiza priključka sa spajalom velikog promjera u ojačanom lameliranom drvu

Prethodno priopćenje

U radu su prikazana istraživanja na priključcima sa spojnim sredstvom promjera 49 mm. Istraživanja su provedena eksperimentalno na dvije grupe uzoraka: uzorcima s lokalnim ojačanjem drva u zoni spoja i bez lokalnog ojačanja. Uzorci su ispitani s unosom sile u spoj okomito na vlakanca drvenog elementa. Svrha provedenih istraživanja je analiza utjecaja količine tkanine na mehaničke karakteristike priključka. Obzirom da su eksperimentalna istraživanja provedena na lokalno ojačanim uzorcima sa 900 g/m^2 tkanine, područje između ojačanih i neojačanih uzoraka nadopunjeno je rezultatima iz parametarske numeričke analize. Za numeričku analizu priključaka metodom konačnih elemenata rabljen je Abaqus/CEA programski paket. Za modeliranje kompleksnih modova otkazivanja, mehaničkih karakteristika i otvaranja pukotine u drvu korištena je UMAT podprogram i kohezijska interakcija između kontaktnih ploha. Rezultati istraživanja pokazali su da primjena tkanine čak i u najmanjoj količini povećava maksimalnu silu i silu popuštanja priključka.

Ključne riječi: *lokalno ojačani drveni spoj, lijepljeno laminirano drvo, mehanička spajala, spajalo velikog promjera, spoj ojačan tkaninom, UMAT podprogram*

1 Introduction

First researches on locally reinforced joints with textile in the connection zone were conducted in 80's of the last century, but since then progress in the textile application for reinforcing timber joints has not been made. Furthermore, locally reinforced joints have not been included in the European timber design code (EC5) [1]. There are few reasons for previously mentioned situation: reinforcing of joints requires additional action in the timber member production process and additional planning and controlling of locally reinforced members through each phase of the manufacturing process.

Proper application of the mechanical fasteners provides timber structures with sufficient rigidity and ductility which can be achieved by applying fasteners of minimum edge and end distance and distance between two adjacent fasteners. Required distance for fasteners recommended by EC5 often requires increasing of elements dimensions at the place of joints. Consequently, that leads to increasing of dimensions of structural members and increasing of the timber volume quantity used per square meter of a structure floor area.

Previously mentioned is applicable on the mechanical fastener 20,0 mm in diameter or smaller. However, if the diameter of the fastener increases above 30,0 mm in diameter, recommended edge and end distance often exceeds the height of the member in which the fastener should be installed. Mentioned problem arises for the mechanical fastener 50,0 mm in diameter, which should be installed into the member 200,0 mm high. For mentioned type of joint, to achieve adequate structural rigidity and ductility, locally reinforced joints have necessary application.

This paper presents the research conducted on the locally reinforced joints with glass fibre textile in the connection zone. Load perpendicular to grain was applied and one mechanical fastener 49,0 mm in diameter was used. Results obtained by experimental tests were used for finite element model (FEM) calibration. Furthermore, with calibrated FEM, parametric analyses were carried out in order to define influence of textile quantity on ductility D and slip modulus k_s of the joint.

This research was carried out with intention to get better insight into the influence of textile quantity on the behaviour of timber joints.

2 State of the art

The first researches that dealt with the reinforcement of timber structural members were carried out on timber beams with reinforced tensile zone, using steel and aluminium rods and strips [2 ÷ 4]. Later studies carried out by Rowland on reinforcing beams using several types of fabrics and glues gave significant results such as increased stiffness and resistance of the beams. The research results also highlighted economic viability of such reinforced timber elements and the possibility of using fabrics as reinforcement at the connection zone [5].

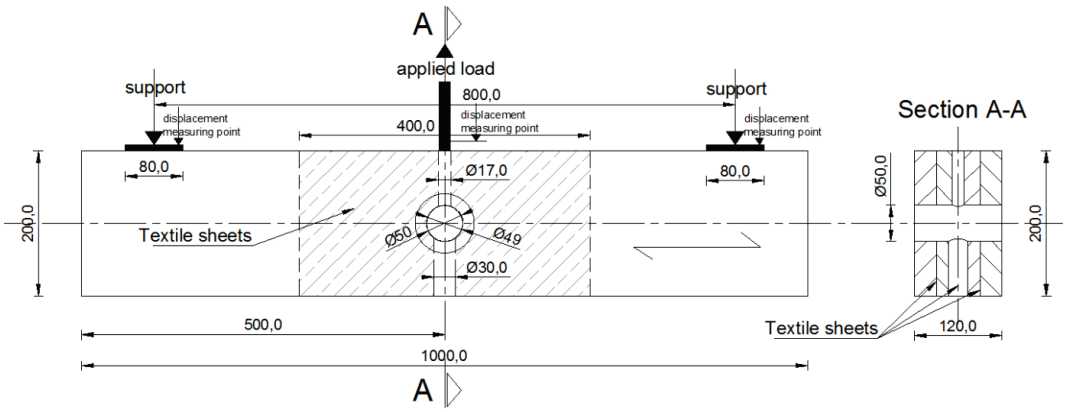

Figure 1 Schematic representation of the timber specimen with boundary conditions

Conducted research was mainly aimed at increasing ductility and reducing the edge and end distance using textile as a reinforcement of a timber element [6 ÷ 8]. Screws, dowels and nails were used for fasteners in these studies.

The research carried out on locally reinforced joints using large diameter mechanical fastener was presented in papers [9, 10]. These studies were conducted using a mechanical fastener 50,0 mm in diameter while the applied load in both studies was parallel to grain. For the above-mentioned studies the textile was specially designed and timber lamellas had grooves for placing the textile.

One of the recent researches with applied load parallel to grain, using a fastener 90,0 mm in diameter, and by screws reinforced timber was presented by Peter Kobel [11].

As was mentioned earlier, design equation for reinforced joints was not included in EC5. Also, EC5 does not contain design equations for larger diameter mechanical fasteners. K. W Johansen in 1949 [12] proposed design equations for fasteners up to 30,0 mm in diameter and since then small changes have been made on these equations which are now implemented in EC5.

Also significant researches were carried out with FEM which at the present stage of software and hardware development obtain results with satisfactory accuracy. Consequently, for timber modelling in papers [13 ÷ 16] major guideline techniques are pointed out.

3 Experimental research

Experimental researches were divided into two groups: specimens with locally reinforced and specimens with non-reinforced timber elements. Four specimens in each group were prepared and tested.

Four lamellas 210,0 mm wide and 32,0 mm thick were glued together with Casco adhesives MUF system 1247/2526 manufactured by Casco adhesives AB, Stockholm, Sweden. Then they were milled in order to obtain samples that were geometrically of the same size, 120,0 mm wide, 200,0 mm high, and 1000,0 mm long.

Specimens for this research were in rotated position for 90°, i.e. with vertically oriented lamellas, which is quite different from traditional laminated timber usage.

Regarding locally reinforced specimens, fibre glass textile sheet 200,0 mm wide and 400,0 mm long was inserted into three adhesive layers. Dimensions of those specimens with the corresponding holes are shown in Fig. 1.

The produced laminated timber was classified as GL 24 h, according to EN 1194.

Material quality used for steel parts was selected according to the stresses obtained from preliminary FEM analyses. Profiled washer, connection bush and tubes were made from steel 42CrMo4 according to EN-10027-2, with ultimate strength f_u =1075,0 N/mm^2 and yield strength f_Y = 925,0 N/mm^2. For elements that were not exposed to stresses like safety rings, steel S235 JRCu with ultimate strength f_u = 535,0 N/mm^2 and yield strength f_Y = 596,0 N/mm^2 was used. Each steel quality group was experimentally tested on specimens. Allen bolt M16 12.9 with mark DIN 912 as part of joint was used for load applying. Glass fiber textile used for reinforcing timber specimens was RT-900 K 2/2, and the fabric weight was 900 g/m^2 ± 5 %.

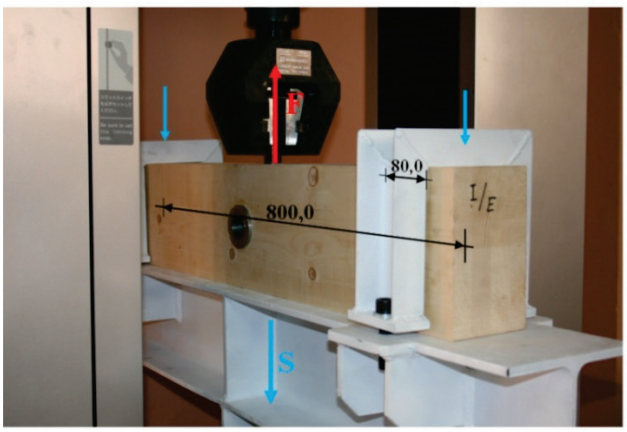

Figure 2 Specimen boundary conditions

Testing of the specimens was conducted on the Shimatzu AG X-300 device (Fig. 2). To achieve boundary conditions of the specimens, steel base device was mounted in the stationary lower jaw of the test machine as shown in Fig. 2. Axial spacing of the supports was 800,0 mm, and each support was 80,0 mm wide.

Tests were carried out by applying a controlled load with a constant rate 5,0 kN/min. When the load reached 25,0 kN, relaxation of 10,0 kN/min followed, until the force of 10,0 kN was reached.

Subsequent to relaxation, constant load with constant rate 5,0 kN/min was applied on the specimens to the failure. During tests every 10,0 s load and displacement

values were recorded. Bolt and supports displacements were recorded during the tests. Difference in recorded displacements between measuring points was compared to the applied load.

During the experiment testing, average humidity value measured in the specimens was 11,5 % ± 1 %, and surrounding temperature was 25 °C ± 1 °C.

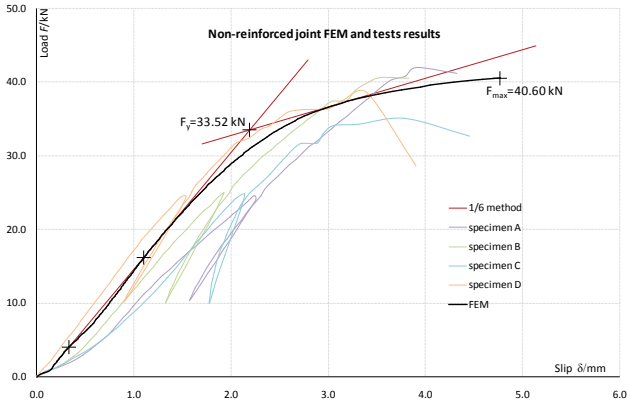

Figure 3 Graphical presentation of non-reinforced joint experimental and FEM results

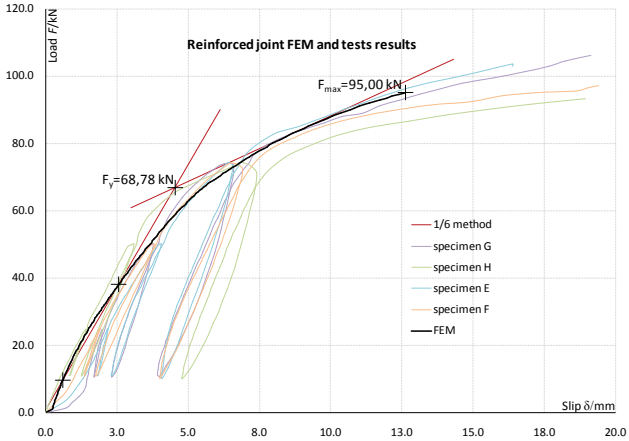

Figure 4 Graphical presentation of reinforced joint experimental and FEM results

Results for each specimen, obtained by experimental tests were analysed by 1/6 method according to EN 12512. In this method yield force F_y is determined by intersection of the following two lines: first line which is determined with point on load-slip curve corresponding to $0{,}1F_{max}$ and point on load-slip curve corresponding to $0{,}4F_{max}$ and second line which is tangent on load-slip curve and has an inclination of 1/6 of the first curve. Two characteristic lines by method 1/6 applied on FEM results are shown in Figs. 3 and 4 (read lines). Furthermore, from represented results in Figs. 3 and 4, joint ductility D and slip modulus k_s were obtained as:

$$D = \frac{\delta_{max}}{\delta_y}, \quad (1)$$

$$k_s = \frac{0{,}4F_{max} - 0{,}1F_{max}}{\delta_{0,4} - \delta_{0,1}}, \quad (2)$$

where F_{max} is maximum force obtained by tests, $\delta_{0,4}$ and $\delta_{0,1}$ are displacements at 40 % and 10 % of maximum force respectively, δ_{max} is displacement at maximum force, and δ_y is displacement at yield force. Main values of mechanical properties obtained by tests are presented in Tab. 1 for non-reinforced specimens and in Tab. 2 for reinforced specimens.

Table 1 Experimental tests results obtained on non-reinforced specimens

Specimens	Specimen A	Specimen B	Specimen C	Specimen D
Slip modulus k_s / kN/mm	13,26	15,24	12,23	17,58
Ductility D / -	1,19	1,33	1,24	1,72
Max. force F_u / kN	42,0	40,65	35,07	38,97

Table 2 Experimental tests results obtained on reinforced specimens

Specimens	Specimen E	Specimen F	Specimen G	Specimen H
Slip modulus k_s / kN/mm	15,73	15,53	20,39	16,34
Ductility D / -	3,13	4,21	4,55	5,11
Max. force F_u / kN	103,65	97,26	106,11	93,28

4 Finite element models

For both groups of specimens FEM were made in the software package ABAQUS/CAE ver. 6.10. Numerical models were created with first-order volume finite elements C3D8 (Figs. 5 and 6). These finite elements are defined with eight nodes and they are using full integration method. For defining non-reinforced timber specimen geometry 25 096 FE was used, and for reinforced timber specimen 39 602 FE. Steel parts in both numerical models were defined with 32 558 FE.

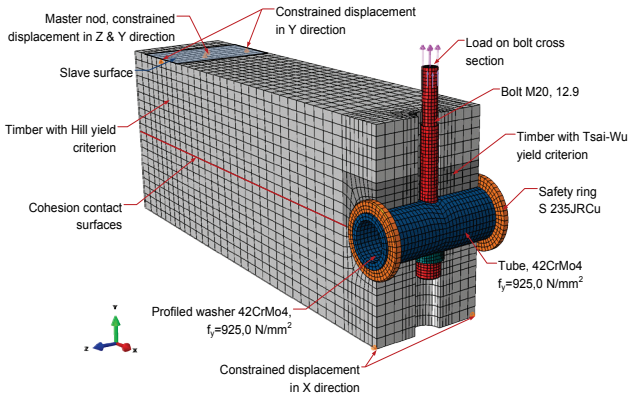

Figure 5 Non-reinforced joint FEM

Boundary conditions for both specimens were defined as presented in Figs. 5 and 6. For supports modelling, master-slave function was used with constrained displacement in Z and Y direction of master nodes. Slave surfaces were defined with mutual centre distance of 800,0 mm, and each surface was 80,0 mm long and 120,0 mm wide. To ensure specimen stabilization five more nodes were constrained in Y and X direction.

Analyses were conducted with Full Newton solution technique, and automatic control of load step increment, while maximum load increment was set to 0,1 N/t. Load

was applied with stress of 6,49612 N/mm^2 on Allan bolt cross section. Applied stress corresponds to the bolt cross section area of 153,0 mm^2 to 1,0 kN.

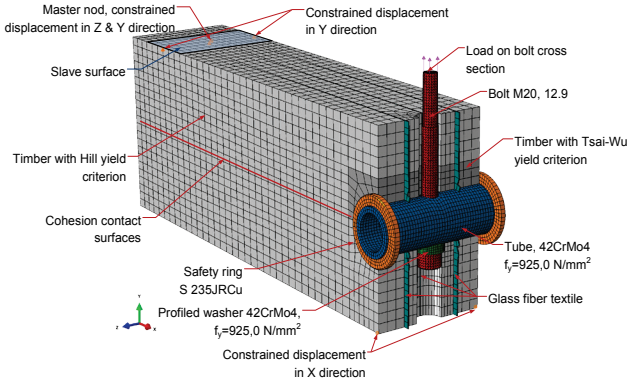

Figure 6 Reinforced joint FEM

For contact modelling between two joint parts, absolute rigidity in the normal direction was used and for tangential direction coefficient of friction 0,2 for steel-steel and 0,25 steel-timber contact was used.[15].

The textile fabric inserted into the adhesive layer for experimental research was modelled using C3D8 volume FE. In order to achieve the accuracy of the FEM, the ratio between the sides of FE was maintained 1:8, using the fabric 1,0 mm thick. For textile sheets, bilinear mechanical behaviour was used (Fig. 7).

Textile specimens were tested for load in warp and weft direction, and average failure loads were obtained P_{u1} = 154,78 N/mm for warp direction and P_{u1} = 161,38 N/mm for weft direction. Failure loads obtained by tests were recalculated to textile ultimate strength for thickness of 1,0 mm. Modulus of elasticity (MOE) E=4 571 N/mm^2, share modulus G= 650,0 N/mm^2, Poisson ratio ν = 0,38 and ultimate strength f_u = 160,0 N/mm^2 were used in FEM for textile sheet.

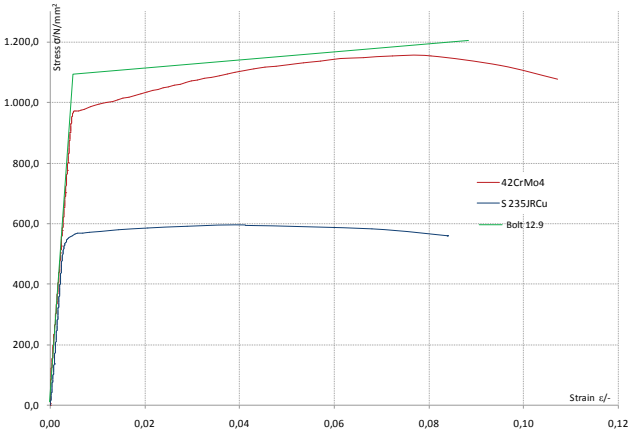

Figure 7 Steel stress-strain diagram

Steel parts in FEM were modelled with elasto-plastic mechanical properties. Mechanical properties E = 210 000 N/mm^2 and ν = 0,3 were used for all steel parts. Steel strength is pointed out in Chapter 3 and stress-strain diagram is shown in Fig 7. For all steel parts except bolt, plastic region was defined thru 17 points, which are corresponding to average stress-strain values obtained from experimental tests. Bolt was modelled as bi-linear with tangential modulus $E_t = E\times 0{,}05$. Steel parts were modelled both in FEM with C3D8 FE defined with eight nodes.

For defining yield criteria and orthotropic elasto-plastic wood behaviour, with different mechanical properties in tension and compression, UMAT subroutine was defined and used. Modified Hill yield criterion [17] was used as the basic wood yield criterion in UMAT subroutine and for timber around fastener Tsai-Wu yield criterion was used.

Tsai-Wu yield criterion can be expressed as:

$$\begin{cases} F_1\sigma_L + F_2\sigma_R + F_3\sigma_T + F_{11}\sigma_L^2 + F_{22}\sigma_R^2 + F_{33}\sigma_T^2 + \\ + F_{44}\tau_{LR}^2 + F_{55}\tau_{LT}^2 + F_{66}\tau_{RT}^2 = 1{,}0 / 0{,}7 / 0{,}0 \\ F_1 = \dfrac{1}{f_{u,L}^t - f_{u,L}^c};\ F_2 = \dfrac{1}{f_{u,R}^t - f_{u,R}^c}; \\ F_3 = \dfrac{1}{f_{u,T}^t - f_{u,T}^c};\ F_{11} = \dfrac{1}{f_{u,L}^t \cdot f_{u,L}^c}; \\ F_{22} = \dfrac{1}{f_{u,R}^t \cdot f_{u,R}^c};\ F_{33} = \dfrac{1}{f_{u,T}^t \cdot f_{u,T}^c}; \\ F_{44} = F_{55} = F_{66} = \dfrac{1}{f_{u,S}^2}. \end{cases} \quad (3)$$

where σ_L, σ_R, σ_T are normal stresses in longitudinal, radial and transversal directions respectively, τ_{RT}, τ_{TL}, τ_{LR} are shear stresses in corresponding planes, $f_{u,L}^t, f_{u,R}^t, f_{u,T}^t$ are wood tensile strengths respectively in longitudinal, radial and transversal directions, $f_{u,S}$ is shear strength, and $f_{u,L}^c, f_{u,R}^c, f_{u,T}^c$ are wood compression strength respectively in longitudinal, radial and transversal directions.

$$\begin{cases} A\cdot(\sigma_R - \sigma_T)^2 + B\cdot(\sigma_T - \sigma_L)^2 + C\cdot(\sigma_L - \sigma_R)^2 + \\ 2D\cdot\tau_{RT}^2 + 2E\cdot\tau_{TL}^2 + 2F\cdot\tau_{LR}^2 \le 1; \\ A = \dfrac{1}{2}\left[\dfrac{1}{(f_{u,R})^2} + \dfrac{1}{(f_{u,T})^2} - \dfrac{1}{(f_{u,L})^2}\right], \\ B = \dfrac{1}{2}\left[\dfrac{1}{(f_{u,T})^2} + \dfrac{1}{(f_{u,L})^2} - \dfrac{1}{(f_{u,R})^2}\right], \\ C = \dfrac{1}{2}\left[\dfrac{1}{(f_{u,L})^2} + \dfrac{1}{(f_{u,R})^2} - \dfrac{1}{(f_{u,T})^2}\right], \\ D = \dfrac{1}{2\cdot(f_{u,RT})^2},\ E = \dfrac{1}{2\cdot(f_{u,TL})^2},\ F = \dfrac{1}{2\cdot(f_{u,LR})^2}. \end{cases} \quad (4)$$

Hill yield criterion [17] expressed by Eq. (4) is modified for compression and for tension separately, because from Eq. (4) arises the following condition: if the stress in one direction reaches yield point, then for the other two directions yield point can be assumed. Much more accurate assumption for tension would be if Eq. (4) was defined for each direction separately. Now, yield criteria for tension are obtained [13, 15] as follows:

$$\frac{\sigma_L^2}{f_{\mathrm{u},L}^{\mathrm{t}\,2}}+\frac{\tau_{LT}^2+\tau_{LR}^2}{f_{\mathrm{u},S}^{\;2}}=1,\quad \frac{\sigma_R^2}{f_{\mathrm{u},R}^{\mathrm{t}\,2}}+\frac{\tau_{LR}^2+\tau_{RT}^2}{f_{\mathrm{u},S}^{\;2}}=1,\quad \frac{\sigma_T^2}{f_{\mathrm{u},T}^{\mathrm{t}\,2}}+\frac{\tau_{LT}^2+\tau_{RT}^2}{f_{\mathrm{u},S}^{\;2}}=1. \tag{5}$$

Yield criterion set by Eq. (5) cannot be applied for compression stresses, because if the yield occurs in wood under compressive stress in one direction, then the yield assumption must be applied on the other two directions.

A yield criterion of maximum principal stress is chosen for wood under compression as follows:

$$\frac{\sigma_L^{\;2}}{f_{\mathrm{u},L}^{\mathrm{c}\,2}}=1,\ \frac{\sigma_R^{\;2}}{f_{\mathrm{u},R}^{\mathrm{c}\,2}}=1,\ \frac{\sigma_T^{\;2}}{f_{\mathrm{u},T}^{\mathrm{c}\,2}}=1. \tag{6}$$

It is important to notice a resemblance between Hill and Hashin yield criterion (1980), which is proposed for materials similar to wood [18]. Eqs. (5) and (6) are implemented in UMAT subroutine for wood yield criterion and they are explained in detail in [19, 20]. Wood elastic mechanical properties and mail ultimate strengths used in FEM and pointed out in Tab. 3, are emanated from laboratory tests which are presented in [19, 21, 22] and literature.

Table 3 Wood material properties and main ultimate strengths

Elastic modulus / MPa	Shear modulus / MPa	Poisson's ratio	Compression strength / MPa	Tension strength / MPa	Share strength / MPa
E_L=11500	G_{LR}=600	ν_{LR}= 0,42	$f_{uL}^{\,c}$= 26,4	$f_{uL}^{\,t}$= 19,8	$f_{u,S}$= 3,3
E_T= 450	G_{RT}=60	ν_{RT}= 0,50	$f_{uT}^{\,c}$= 2,97	$f_{uT}^{\,t}$= 0,38	
E_R= 600	G_{LT}=650	ν_{LT}= 0,48	$f_{uR}^{\,c}$= 2,97	$f_{uR}^{\,t}$= 0,38	

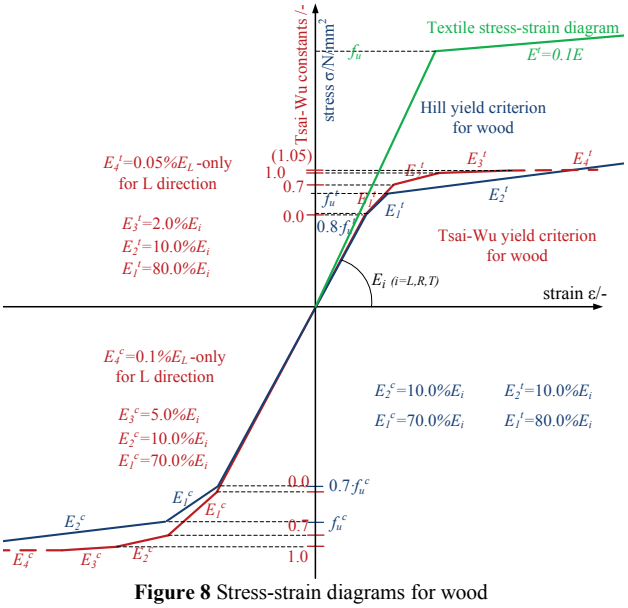

Figure 8 Stress-strain diagrams for wood

Also, for defining mechanical properties of textile sheets, UMAT subroutine was used. Because glass fibre textile in compression has no strength, it can be assumed that mechanical properties of wood with Tsai-Wu criterion can be applied on textile under compression. For textile in tension, maximum principal stress criterion was used.

Along with UMAT subroutine, surface-based cohesive behaviour was used for defining crack opening in wood. Surface-based cohesive behaviour is very similar to the cohesive elements with traction-separation response [23] and is defined by interfacial penalty stiffness E_i^0 (i = 1, 2, 3, normal, the first, and the second shear direction, respectively), interfacial strength σ_i^0, and critical fracture energy G_i^{c}. Fig. 9 shows traction separation law, which consists of elastic deformation, damage initiation criterion and linear damage evaluation law. Prior to the initiation of damage, elastic deformation will be produced and can be expressed as:

$$\delta_i^0=\frac{\sigma_i^0}{E^0};\quad i=1,2,3. \tag{7}$$

Interfacial penalty stiffness is taken as E^0 =20 000 N/mm and it is not material-related parameter. Damage initiation starts when the contact stresses satisfy a specified damage initiation criterion. In this case quadratic nominal stress criterion is used for damage initiation, and it is defined by Eq. (8).

$$1=\left\{\frac{\langle\sigma_1\rangle}{\sigma_1^0}\right\}^2+\left\{\frac{\sigma_2}{\sigma_2^0}\right\}^2+\left\{\frac{\sigma_3}{\sigma_3^0}\right\}^2, \tag{8}$$

where $\langle\sigma_1\rangle$ indicates that a pure compression stress state will not initiate damage. Total deformation for cohesion elements until crack appears can be expressed as follows:

$$\delta_{\mathrm{m}}=\sqrt{\langle\delta_1^2\rangle+\delta_2^2+\delta_3^2}. \tag{9}$$

Assuming that two shear directions have equal mechanical properties, expression for the crack deformation can be expressed as follows [24, 25]:

$$\delta_2^0=\delta_3^0=\delta_{\mathrm{pos}}^0;\quad \beta=\frac{\delta_{\mathrm{pos}}}{\delta_1};$$
$$\delta_m^0=\begin{cases}\delta_1^0\delta_2^0\sqrt{\dfrac{1+\beta^2}{\left(\delta_2^0\right)^2+\left(\beta\cdot\delta_1^0\right)^2}} & \leftarrow\delta_1^0>0\\ \delta_{\mathrm{pos}}^0 & \leftarrow\delta_1^0\le 0\end{cases}. \tag{10}$$

Using corresponding energy release values shown in Fig. 9, total deformation at complete failure can be expressed for specific directions as follows:

$$\delta_i^{\mathrm{f}}=\frac{2\cdot G_i^{\mathrm{c}}}{\sigma_i^0};\quad i=1,2,3. \tag{11}$$

Mixed-mode fracture energy dependence can be defined by a power law fracture criterion. Power law criterion states that failure under mixed-mode condition is

governed by the interaction of the energies required to cause failure in the individual modes.

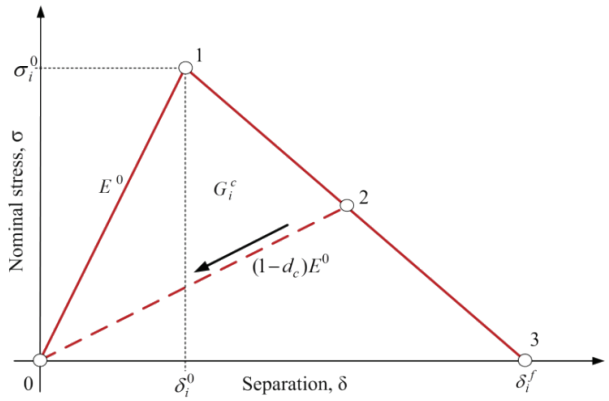

Figure 9 Bilinear constitutive model for crack opening

Criterion can be written as follows:

$$\left\{\frac{G_1}{G_1^{\mathrm{c}}}\right\}^{\alpha}+\left\{\frac{G_2}{G_2^{\mathrm{c}}}\right\}^{\alpha}+\left\{\frac{G_3}{G_3^{\mathrm{c}}}\right\}^{\alpha}=1. \tag{12}$$

In Eq. (12) quantities G_1, G_2, G_3 refer to work done by the traction and conjugate relative displacement in normal and two share directions. Quantities G_1^{c}, G_2^{c}, G_3^{c} need to be specified, and they refer to critical energies required to cause failure in certain direction.

From the above mentioned the following equation for the total deformation at complete failure can be expressed by the dissipated energy criterion:

$$\delta_{\mathrm{m}}^{\mathrm{f}}=\begin{cases}\dfrac{2\left(1+\beta^2\right)}{E^{\mathrm{c}}\delta_{\mathrm{m}}^0}\cdot\left[\left\{\dfrac{1}{G_1^{\mathrm{c}}}\right\}^{\alpha}+\left\{\dfrac{\beta^2}{G_2^{\mathrm{c}}}\right\}^{\alpha}\right]^{\frac{-1}{\alpha}} & \leftarrow \delta_1^0>0\\ \delta_{\mathrm{pos}}^k & \leftarrow \delta_1^0\le 0\end{cases}. \tag{13}$$

Constitutive equations for the mixed-mode failure are defined with interfacial penalty stiffness E, crack opening function d and total crack deformation $\delta_{\mathrm{m}}^{\mathrm{f}}$, δ_{m}^0, and can be expressed as follows:

$$\sigma=D_{sr}\delta_r, \tag{14}$$

$$D_{sr}=\begin{cases}\overline{\delta_{sr}}E^0 & \leftarrow \delta_{\mathrm{m}}^{\max}\le\delta_{\mathrm{m}}^0\\ \overline{\delta_{sr}}\left[\left(1-d\right)E^0+E^0 d\,\overline{\delta_{s1}}\dfrac{\langle-\delta_1\rangle}{-\delta_1}\right] & \leftarrow \delta_{\mathrm{m}}^0\le\delta_{\mathrm{m}}^{\max}\le\delta_{\mathrm{m}}^k\\ E^0\overline{\delta_{s1}}\overline{\delta_{1r}}\dfrac{\langle-\delta_1\rangle}{-\delta_1} & \leftarrow \delta_{\mathrm{m}}^{\max}\le\delta_{\mathrm{m}}^k\end{cases}, \tag{15}$$

$$d=\frac{\delta_{\mathrm{m}}^{\mathrm{f}}\left(\delta_{\mathrm{m}}^{\max}-\delta_{\mathrm{m}}^0\right)}{\delta_{\mathrm{m}}^{\max}\left(\delta_{\mathrm{m}}^{\mathrm{f}}-\delta_{\mathrm{m}}^0\right)},\ d\in[0,1] \tag{16}$$

Mechanical properties for cohesion contact surfaces are taken from literature [26] and they are presented in table Tab. 4.

Table 4 Surface-based cohesive behaviour mechanical properties

	Timber	Textile	Adhesive
G_1^{c}	0,179	1,0	4,0
G_2^{c}	0,4	3,0	6,0
G_3^{c}	0,4	3,0	6,0
E^{c}	1000,0	4500,0	10000,0
α	1,0	1,0	1,0

5 Results obtained by FEM

FEM results of reinforced joint with 900,0 g/m^2 of glass fibre textile in connection zone and non-reinforced joint were analysed by 1/6 method according to EN12512 norm. Obtained FEM results are presented together with experimental tests results in Fig. 3 and Fig. 4. Presented results show good overlapping in load-slip curve and small variations between tests and FEM results. Good overlapping between results is important if we bear in mind that the same FEM were used for the parametric analyses.

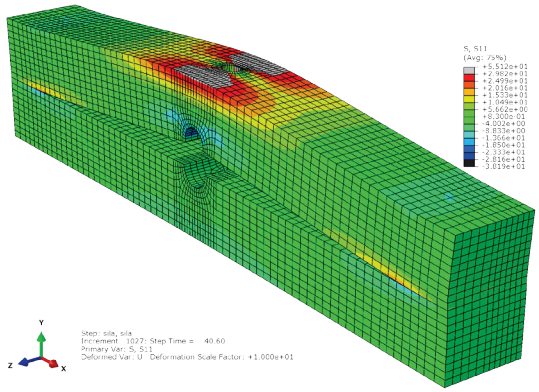

Figure 10 Stresses in direction S11 - non-reinforced specimen

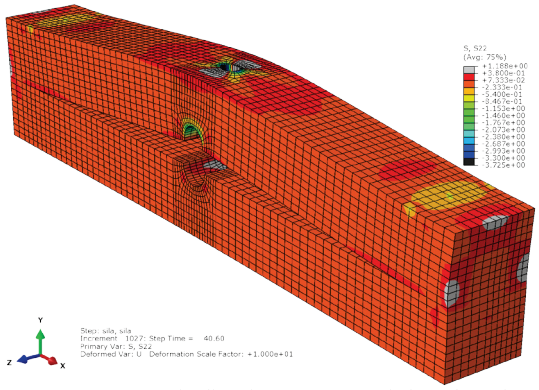

Figure 11 Stresses in direction S33 - non-reinforced specimen

The biggest difference between FEM results and experimental tests results are noticed in the strains above yield force of the reinforced joint. In experimental tests after embedding compression strength in timber specimens was reached, strains propagation increased, and the fastener sank into the timber. With Tsai-Wu yield criterion previously mentioned mode failure has been successfully obtained with FEM but with small variation. The reason for this difference is inability to accurately

numerically define descending branch in the wood stress-strain diagram in compression.

Stresses parallel (S11) and perpendicular to grain (S33) at the time of joint failure are presented in Figs. 10, 11, 14 and 15. At the time of complete joint failure, stresses parallel to grain were between the compression and tension yield stresses.

Exceeding of embedding compression strength is visible in reinforced specimen shown in Fig.15 (stresses perpendicular to grain).

Tensile stress perpendicular to grain caused initial cracks in the middle of the timber specimen. Complete failure was caused by interaction of tensile and shear stresses parallel to grain. The stresses in the cohesion zone in the time of specimen failure are shown in Fig. 12 and Fig. 13.

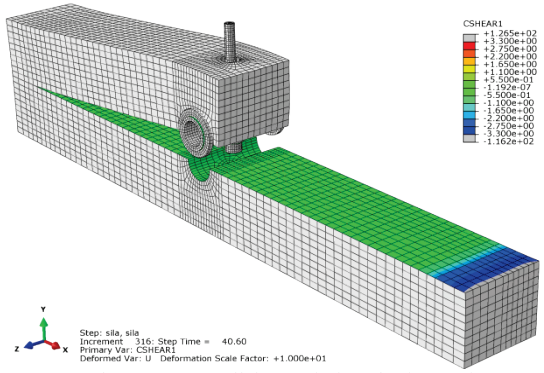

Figure 12 Shear stress parallel to grain in cohesion surface, non-reinforced specimen

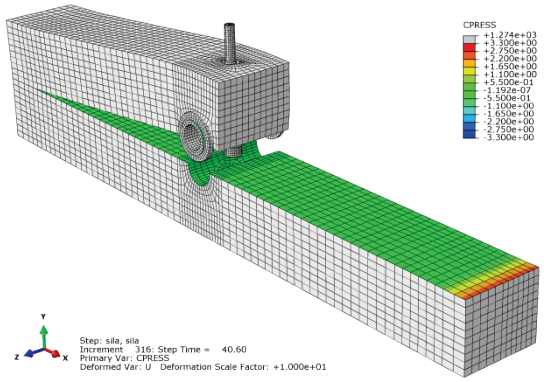

Figure 13 Normal stress perpendicular to grain in cohesion surface - non-reinforced specimen

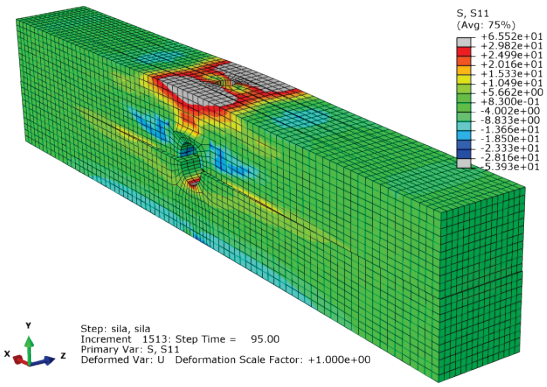

Figure 14 Stresses in direction S11 - reinforced specimen with 900,0 kg/m^2 of textile

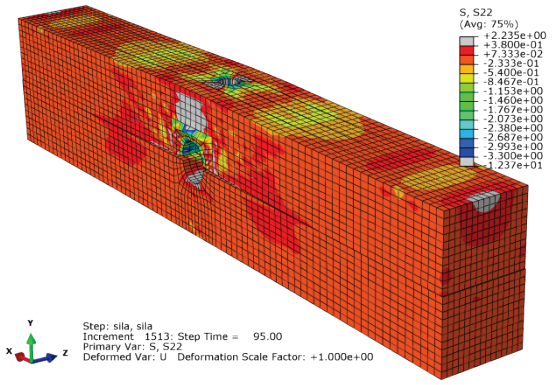

Figure 15 Stresses in direction S33 - reinforced specimen with 900,0 kg/m^2 of textile

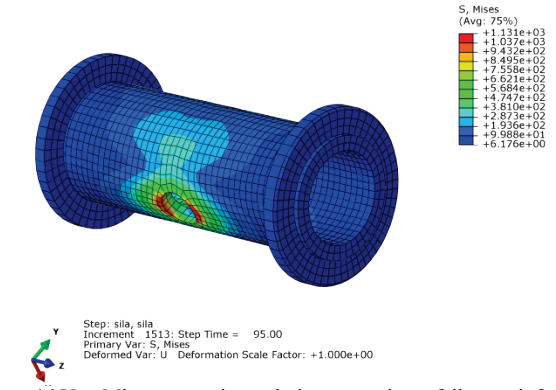

Figure 16 Von Misses stress in steel pipe at specimen failure, reinforced specimen with 900,0 kg/m^2 of textile

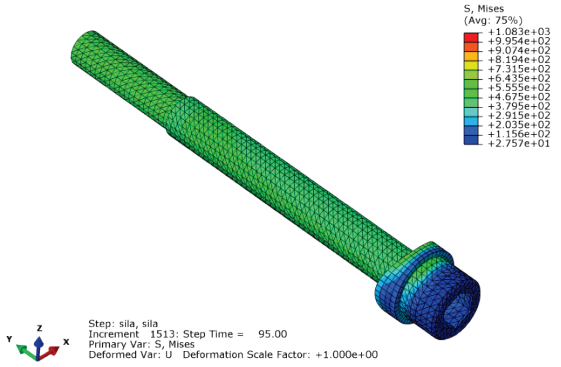

Figure 17 Von Misses stress in bolt at specimen failure, reinforced specimen with 900,0 kg/m^2 of textile

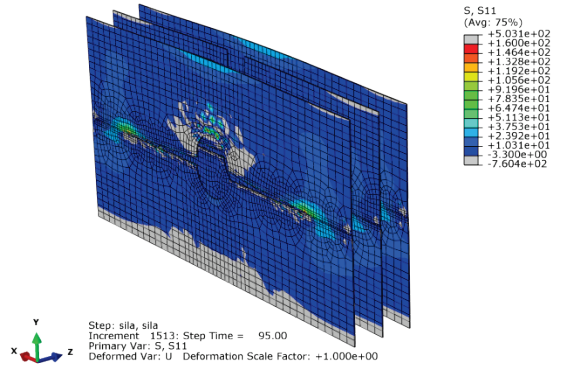

Figure 18 Stresses in textile in direction S11 (warp direction) reinforced specimen with 900,0 kg/m^2 of textile

The main purpose of FEM research was to calibrate material mechanical properties and mode failures.

Calibrated FEM's were used for making parametric FEM analyses.

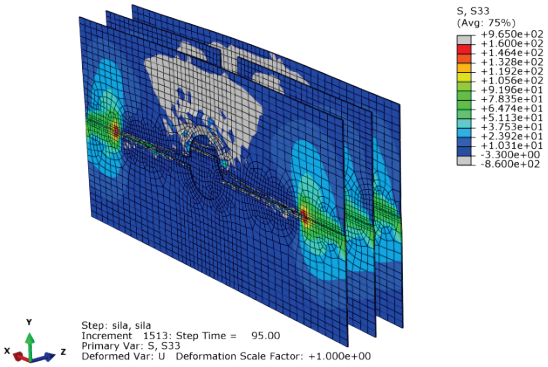

Figure 19 Stresses in textile in direction S22 (weft direction) reinforced specimen with 900,0 kg/m^2 of textile

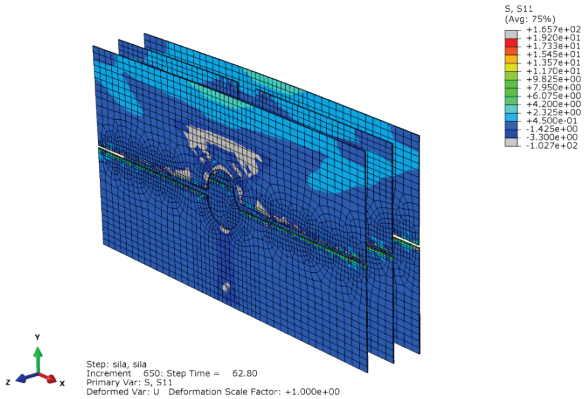

Figure 20 Stresses in textile in direction S11 (warp direction) reinforced specimen with 108,0 kg/m^2 of textile

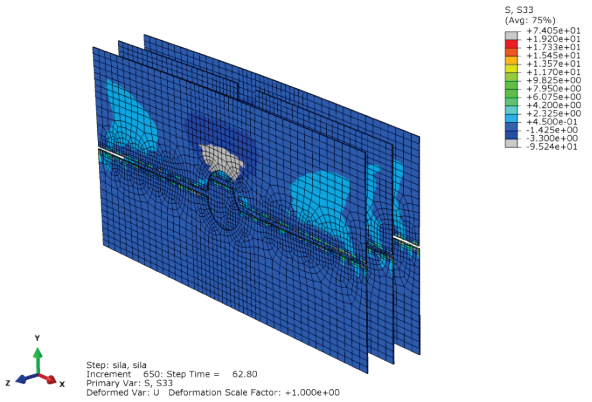

Figure 21 Stresses in textile in direction S22 (weft direction) reinforced specimen with 108,0 kg/m^2 of textile

Table 5 Parametric FEM results

Textile quantity m / g/m^2	DOR μ / kg/(m^2·m)	Maximal force F_u / kN	Strength f_h / N/mm^2	Yield force F_y / kN	Stiffness K_s / kN/mm
900,0	22,50	95,0	16,711	66,97	14,47
450,0	11,25	84,0	14,78	62,89	15,46
225,0	5,625	70,8	14,40	52,44	16,34
108,0	2,70	62,8	12,62	46,28	16,82
0,0	0,0	40,6	7,47	33,49	15,82

Parametric FEM analyses were carried out on the reinforced joint with the following quantities for the textile in place of connection: 450,0 g/m^2, 225,0 g/m^2 and 108,0 g/m^2. Results of numerical analyses are presented in slip-load graphs for each model separately (Figs. 22 ÷ 26). All results obtained by parametric FEM (Tab. 5) were analysed by 1/6 method according to EN12512 norm.

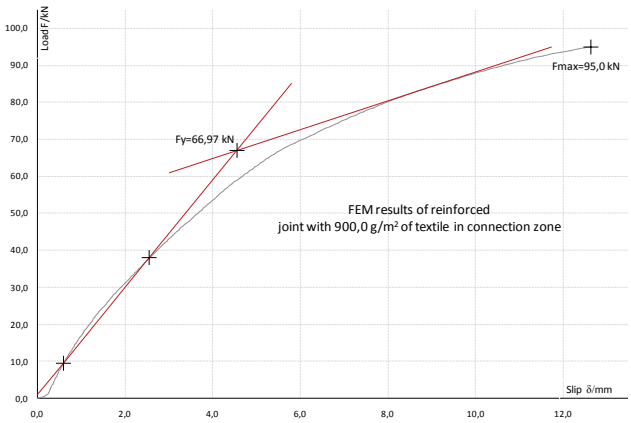

Figure 22 FEM results of reinforced joint with 900,0 g/m^2 of textile in connection zone

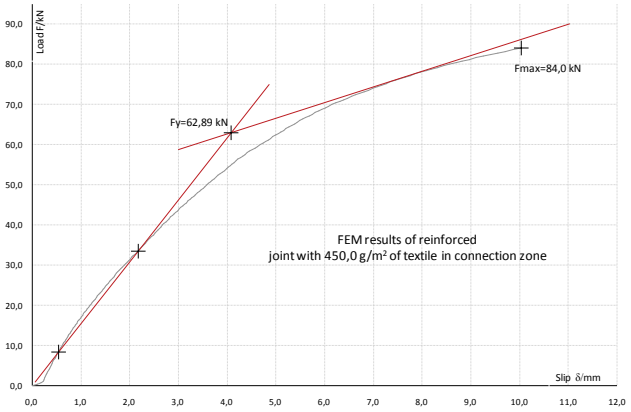

Figure 23 FEM results of reinforced joint with 450,0 g/m^2 of textile in connection zone

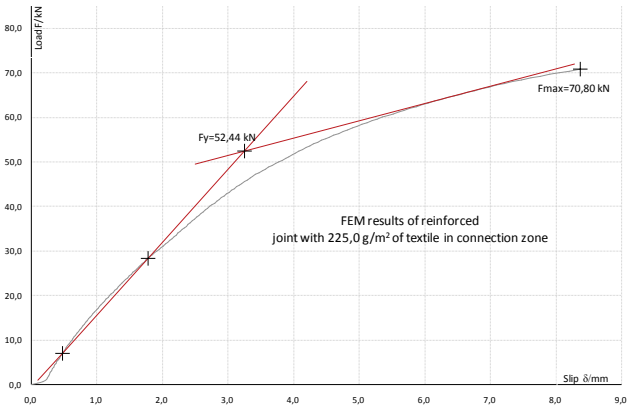

Figure 24 FEM results of reinforced joint with 225,0 g/m^2 of textile in connection zone

In Tab. 5 given values were calculated using the following equations:

$$\mu = \frac{\sum m}{A \cdot t} - \text{degree of reinforcement (DOR)}, \quad \frac{\text{kg}}{\text{m}^2 \cdot \text{m}}$$

where Σm is total textile mass in joint, A is timber reinforced surface in specimen and t is timber specimen thickness.

$$f_{\mathrm{h}} = \frac{F_{\mathrm{u}}}{A_{\mathrm{f}}} - \text{ultimate strength},$$

where A_{f} is fastener contact surface.

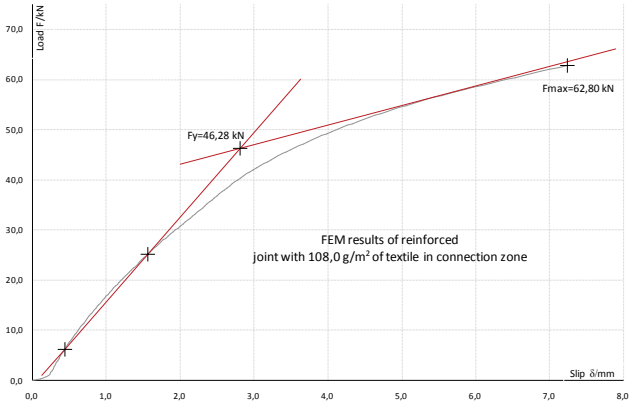

Figure 255 FEM results of reinforced joint with 108,0 g/m^2 of textile in connection zone

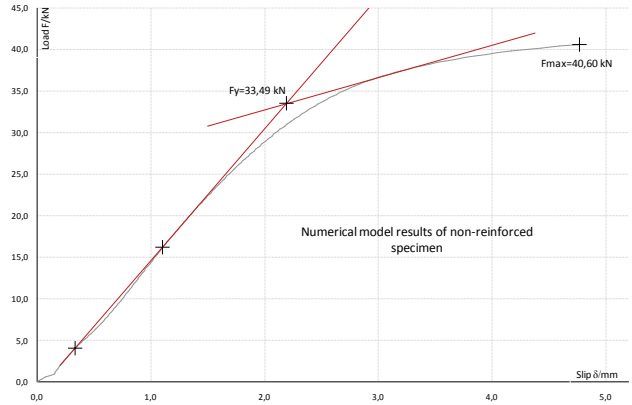

Figure 26 FEM results of non-reinforced joint

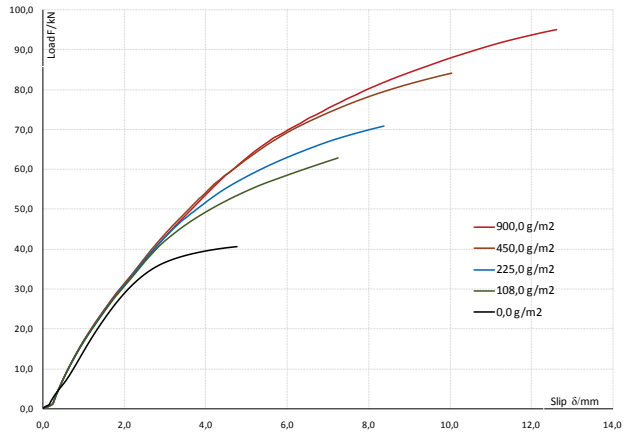

Figure 27 FEM results obtained by parametric analyses

6 Conclusion

Research results have shown that glass fibre textile placed between lamellas in adhesive layer effectively increases the resistance of the timber element as well as the tensile strength of laminated timber perpendicular to grain. In locally reinforced joints maximum force and yield force have doubled and the ductility has increased 3,24 times comparing to non-reinforced joints, which economically justifies this way of reinforcing timber structures.

FEM with complex mechanical characteristics of timber, crack opening and propagation, presented in this paper, showed good correlation with experimental results. Such complex numerical models provide realistic behaviour of joints and were used to determine the influence of textile quantity on the joint resistance.

FEM results have shown that the resistance of the joint does not increase linearly with an increasing of textile quantity, and thus the economic profitability of reinforced joint is limited.

7 References

[1] European Committe for Stardardization (CEN). BS EN1995-1-1:2004. Eurocode 5 - Design of timber structures. Part 1-1: General - Common rules and rules for buildings: CEN. Brussels, Belgium; 2004.

[2] Bohannan, B. Prestressed laminated wood beams. Madison, WIS: U.S. Forest service; 1964.

[3] Mark, R. Wood-aluminium beams within and beyond the elastic range. // Forest Products Journal. 11, (1961), pp. 477-484.

[4] Borgin, K. B.; Loedolff, G. F.; Saunders, G. S. Laminated Wood Beams Reinforced with Steel Strips. // ASCE Journal of the Structural Division. 94, (1968), pp. 1681-1706.

[5] Rowland, R. E.; Van Dewegh, R. P.; Laufenber, T. L.; Kruege, G. P. Fiber-reinforced wood composites. // Wood and Fiber Science. 18, (1986), pp. 39-57.

[6] Chen, C-J. Mechanical Behavior of Fiberglass Reinforced Timber Joints. Ph.D. Thesis No. 1940. Lausanne, Switzerland: Swiss Federal Institute of Technology, Lausanne, EPFL, 1999.

[7] Chen, C. J.; Lee, T. L.; Jeng, D. S. Finite element modeling for the mehanical behavior of dowel-type timber joints. // Computers and Structures. 81, (2003), pp. 2731-2738.

[8] Windorski, D. F.; Solits, L. A.; Ross, R. J. Feasibility of Fiberglass-Reinforced Boltes Wood Connections. Madison, WI: U.S. Department of Agriculture: Forest Service, Forest Products Laboratory, 1997, p. 9.

[9] Haller, P.; Birk, T.; Offermann, P.; Cebulla, H. Fully fashioned biaxial weft knitted and stitch bonded textile reinforcements for wood connection. // Composites: Part B. 37, (2006), pp. 278-285.

[10] Heiduschke, A.; Haller, P. Performance of composite - reinforced timber joints using single dowel-type. / World Conference on Timber Engineering. Miyazaki, Japan, 2008, pp. 1140-1148.

[11] Kobel, P. Modelling of Strengthened Connections for Large Span Truss Structures. Master's Thesis, Department of Structural Engineering, Lund Institute of Technology, Sweden, 2011.

[12] Johansen, K. W. Theory of timber connections. Association for Bridge and Structural Engineering. Zurich, Switzerland, 1949, pp. 249-262.

[13] Xu, B-H.; Bouchair, A.; Taazount, M. 3D Non-linear Finite Element Modelling of Traditional Timber Connections. World conference on timber engineering. Riva de Garda, Trento, Italy, 2010, pp. 3302-3309.

[14] Kharouf, N.; McClure, G.; Smith, I. Elasto-plastic modeling of wood bolted connections. // Computers and Structures. 81, (2003), pp. 747-754.

[15] Xu, B. H.; Bauchair, M.; Taazount, M.; Vega, E. J. Numerical and experimental analyses of multiple-dowel steel-to-timber joints in tension perpendicular to grain. // Engineering Structures. 31, (2009), pp. 2357-2367.

[16] Guan, Z. W.; Zhu, E. C. Finite element modelling of anisotropic elasto-plastic timber beams with openings. // Engineering Structures. 31, (2009), pp. 394-403.
[17] Hill, R. A Theory of the yielding and plastic flow of anisotropic metals. // Proceedings the royal society A. 193, (1984), pp 281-297.
[18] Hashin, Z. Failure Criteria for Unidirectional Fiber Composites. // Journal of Applied Mechanics. 47, (1980), pp. 329-334.
[19] Pavković K. Hybrid joint of timber truss girders. PhD Thesis, Faculty of civil engineering, University of Zagreb, Zagreb. 2013.
[20] Pavković, K.; Haiman, M.; Meštrović, M.; Rajčić, V. Truss girder joint with a large diameter mechanical fastener. // Građevinar. 65, (2013), pp. 869-878.
[21] Haiman, M. Safety analysis of laminated members. PhD Thesis, Faculty of Civil Engineering, University of Zagreb, Zagreb, 2001.
[22] Čizmar, D. Structural robustness of timber truss girder. PhD Thesis, Faculty of Civil Engineering, University of Zagreb, Zagreb, 2012.
[23] Abaqus. Analysis User's Manual Volume V: Prescribed Conditions, Constraints & Interactions 6.10.
[24] Camanho, P. P.; Davila, C. G. Mixed-Mode Decohesion Finite Elements for the Simulation of Delamination in Composite Materials. NASA/TM-2002-211737, 2002.
[25] Elmarakbi, A. Finite Element Analysis of Delamination Growth in Composite Materials using LS-DYNA: Formulation and Implementation of New Cohesive Elements. // Advances in Composites Materials. 2011, pp. 409-428. (www.intechopen.com)
[26] Haller, P.; Putzger, R. Fracture Energy in Mode I and Mode II of Reinforced Wood. Dresden, Germany: Department of Civil Engineering, Technische Universität Dresden; 2006. p. 4.

Authors' addresses

Krunoslav Pavković, PhD MSc CEng
Department of Civil Engineering, Polytechnic of Zagreb
Av. Većeslava Holjevca 15, 10010 Zagreb, Croatia
E-mail: krunoslav.pavkovic@tvz.hr

Vlatka Rajčić, Full Professor, PhD MSc CEng
Faculty of Civil Engineering, University of Zagreb
Fra A. Kačića-Miošića 26, 10 000 Zagreb, Croatia
E-mail: vrajcic@grad.hr

Dean Čizmar, PhD MSc CEng
Department of Civil Engineering, Polytechnic of Zagreb
Av. Većeslava Holjevca 15, 10010 Zagreb, Croatia
E-mail: dean.cizmar@tvz.hr